Periodicals of Engineering and Natural Sciences ISSN 2303-4521
Vol. 8, No. 3, September 2020, pp.1288-1296

Effects of holes radius on plasmonic photonic crystal fiber sensor with internal gold layer

Muayad H. Salman[1], Haider K. Muhammad[2], Hassan A. Yasser [3]
[1] Imam AL-Kadhim University College, Baghdad, Iraq
2 Physics Department, Education College, Thi-Qar University
3 Physics Department, Science College, Thi-Qar University

ABSTRACT

In this study, a plasmonic photonic crystal fiber (PCF) sensor was designed with an internal gold layer between the liquid holes and the air holes. The study shown that the thickness of the gold layer, the radius of the air holes and the radius of the liquid holes all have a significant effect on the sensitivity of the sensor, where a wavelength sensitivity of (10,500 nm/RIU) was achieved at certain simulation conditions. Under these chosen conditions, the relationship of resonance wavelength with the refractive index of the liquid was linear and this gives flexibility to extend the range of the refractive index of the analyte without changing the sensor design. Approaching or moving away of the holes from center in the proposed design has a fundamental role in determining the sensor characteristics.

Keywords: Fiber Optics, Plasmonic photonic crystal fiber, Optical sensing and Sensors, Sensitivity.

Corresponding Author:

Muayad H. Salman
Imam AL-Kadhim University College
Baghdad, Iraq
E-mail: moedh@alkadhum-col.edu

1. Introduction

Over the last few decades, photonic biosensors have very attracted intense attention because of their promising applications in many fields including medical diagnostics, environment monitoring, organic chemical detection, temperature, magnetic fields, etc. [1,2]. A large number of optical fiber sensors have been developed based on several techniques such as resonant mirror, fiber Bragg grating, microring resonator, and Surface plasmon resonance (SPR) considered one of the most important techniques. The last technique is a prominent optical phenomenon, involving resonant excitation of electromagnetic surface waves in combination with collective free electron oscillations in metal[3,4], the oscillations of collective charge at the metal-dielectric interfaces known as plasmonics surface waves (PSWs) can be easily guided and generated by coupling the electromagnetic field into charge-density particles of noble metals such as gold (Au), silver (Ag), copper (Cu), aluminum (Al), etc. Along the interface of the metal-dielectric in the form of a traveling wave known as surface plasmon polariton (SPP) [5,6], creation the phase matching state between the SPP mode and the optical fiber-core guided mode at a given wavelength and fast response, accordingly, surface plasmons resonance (SPR) are promising, effective optical detection approach for the study of label free bio-molecular interactions in real time by label free sensing in a variety of bio-medical applications, and extremely sensitive to changes in the refractive index of the dielectric [7,8], hence, with changing analyte RI, the resonance wavelengths are shifted to lower or higher wavelength, so that the analyte can be properly detected [9].
Noticeably, PSWs are excited by the evanescent fields present on a prism surface at complete internal reflection [10], on that perspective, that requires bulky components and restricts the use of such instrument to laboratory environment [6]. Using optical fibers instead of the prism has opened the way towards remote sensing applications based on SPR, with the advent and development of photonic optical fiber technology, a new era of optical sensing has emerged [11], which has the ability to solve all previous difficulties, where it is distinguished

by many important features such as low propagation loss, compact size, high degree of integration, geometrical flexibilities real-time detection ability, high sensitivity, etc. [11,12].
In this paper, a PCF based SPR-RI sensor is proposed. The performance of the proposed sensor is investigated using software COMSOL based on finite element method (FEM) with perfectly matched layer (PML). The main objective is to maximize and improve sensitivity

2. Sensor design

The schematic of the proposed FCF based SPR sensor is shown in Figure 1. The model consists of two rings of holes, where the inner contains six analyte holes with a radius R_1. The holes spaced from each other by distance Λ_1. The center of each circle is away from the sensor center by the distance r_1. The outer ring consists of eight air holes with radius R_2 that spaced from each other by distance Λ_2. The distance between the center of each of them to the sensor center is r_2. The radius of sensor extends to r_4. Thereafter, the PML layer will be presented, to complete the sensor design, a gold layer with t_m thickness and r_3 radius will putting between the two rings of holes. Note that, air holes are made with a large radius to ensure the waveguide idea.
In this work, we select Gold (Au) because of its distinctive properties, as an chemically noble metal, stable, does not suffer from oxidization, and has high resonance peak shifts compared to other active plasmonic materials like Ag, Cu and Al, etc., so a layer of Au with a different thickness are used to improve the sensing performance.

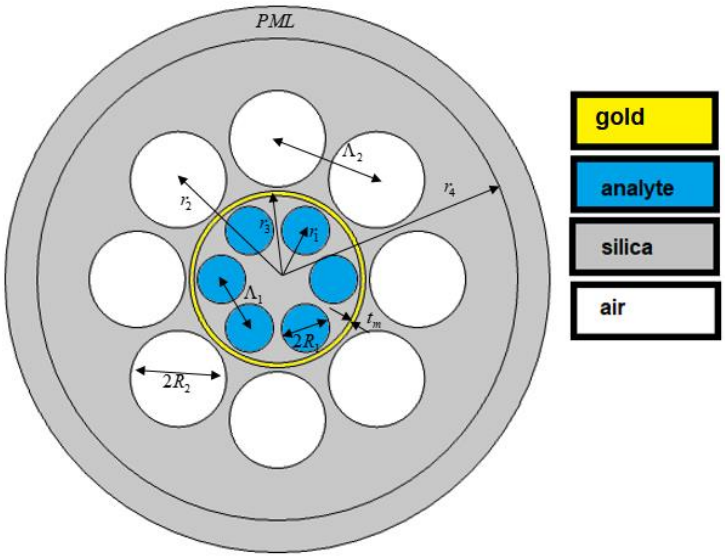

Figure 1. The proposed structure of sensor

Table 1. the definitions of sensor parameters

parameter	specification	parameter	Tested value
r_1	h	h	**(3.5, 3.6, 3.7)** μm
Λ_1	h	$R1$	**(1.4,1.5,1.6)** μm
r_2	3.5 h	R_2	**(3,3.15,3.3)** μm
Λ_2	3.5 h	r_4	**15** μm
r_3	1.486 h	t_m	***(80,100,120) nm***

3. Theoretical aspects

The structure of the proposed sensor is made of silica essentially, all the holes in the structure is empty i.e., air filled. So the refractive index of the silica is determined by the Sellmeier equation [13]

$$n^2(\lambda) = 1 + \frac{A_1 \lambda^2}{\lambda^2 - B_1} + \frac{A_2 \lambda^2}{\lambda^2 - B_2} + \frac{A_3 \lambda^2}{\lambda^2 - B_3} \quad (1)$$

where, n is the refractive-index of silica, λ is the operating of the wavelength in the micrometer unit and A1, A2, A3, B1, B2,and B3 are Sellmeier coefficient available at Ref [12].
Drude model at higher frequency regime is not suitable for calculating the real and imaginary part of dielectric constant (ε). This problem can be nullified by introducing the interband (IB) effect as a sum of Lorentzian functions, One can easily express the dielectric function dependent on the frequency as $\varepsilon(\omega) = \varepsilon_{Drude}(\omega) + \varepsilon_{IB}(\omega)$ [14,15]. So, according to the Drude-Lorentz model, the material dispersion of Au as the noble metal could be expressed as [16]

$$\varepsilon_{Au} = \varepsilon_{\infty} - \frac{\omega_D^2}{\omega(\omega + j\gamma_D)} - \frac{\Delta\varepsilon\,\Omega_L^2}{(\omega^2 - \Omega_L^2) + j\Gamma_L\omega} \quad (2)$$

where, ε_{Au} refers to the permittivity of Au, ε_{∞} is the permittivity at a high frequency which its value of 5.9673. Also, ω , ω_D and $j\gamma$ are the angular frequency , the frequency of the plasma and the frequency of the damping, respectively. Moreover, $\gamma_D/2\pi = 15.92\,THz$, $\omega_D/2\pi = 2113.6\,THz$, and weighting factor is $\Delta\varepsilon = 1.09$. The Lorentz-oscillators strength and the width of the spectral are given by $\Omega_L/2\pi = 650.07\,THz$ and $\Gamma_L/2\pi$ =104.86 THz, respectively. The measurements of these optical data are heavily dependent on the experimental conditions, so the relevant optical data must be selected carefully.
According to the mechanism of the phase matching between SPP and core modes were generated, the peaks of the loss are forming where the coupling occurs [2]. The confinement loss is a measurement to any change at the phase matching period. Therefore, The confinement loss is used by wavelength or spectral interrogation methods as a main source to detect changes on analyte, i.e. the unknown analyte can be detected from the resonant wavelength shifts or from the loss peaks of the amplitude variation, The confinement loss is calculated by using the expression as stated in [17,18].

$$\alpha_{loss}(dB/cm) \approx 8.686 \times k_0\, Im\{n_{eff}\} \times 10^4 \quad (3)$$

where Im{n_{eff}} indicates the effective refractive index of the imaginary part and $k_0 = 2\pi/\lambda$ and λ are the wave vector of free space and the operating wavelength in micrometer unit, respectively. Essentially The plasmonic PCFs sensors are operated in the wavelength interrogation mode. So, change in the all values are detected by measuring the shift of absorption loss peak that will occur due to SPR phenomenon, there are two important main methods used, the first is a spectral- based defined as [3]

$$S(\lambda)(nm/RIU) = \frac{\partial\lambda_{peak}}{\partial n_a} \quad (4)$$

where $\partial\lambda_{peak}$ and ∂n_a are the difference of wavelength length between two loss curves for two adjacent RI of analytes (na) and RI of analytes difference. Noticeably, in this work has been taken ($\partial n_a = 0.01$). The second detection approach, considering as another performance quantifying parameter of the biosensor which depends on RI contrast of the core-cladding, the amplitude-based method of detection can be given as [19,20]

$$S(\lambda)(RIU^{-1}) = -\frac{1}{\alpha(\lambda, n_a)}\frac{\partial\alpha(\lambda, n_a)}{\partial n_a} \quad (5)$$

where ∂n_a refers to the difference of loss between two consecutive RI analyte and $\alpha(\lambda, n_a)$ is the propagation loss of the core mode as a function of the operating wavelength.

4. Results and discussion

All simulations are performed using the values: h = 3.5 μm, R_1 =1.5μm, R_2 =3μm, t_m = 80nm, r_4 =15μm and will be indicated in time when a change occurs. The COMSOL environment was used to determine the relation between wavelength and effective refractive index, where this software uses finite element method (FEM) that is built on the basis of dividing the cross section into small parts and forming the mesh. The type and accuracy of the mesh are chosen in order to achieve better accuracy with a suitable operating time for the computer.
Figure 2 represents the relationship of the loss with the wavelength of the refractive indices of the analyte (n_a =1.37, 1.38, 1.39, 1.40) using several values of the factor h. It is clear from the figure that there are approximately two peaks for each na value for all states h within the wavelength range (1.9-2.3 μm), but in the

case (h =3 μm) we notice that the first set of values is separated from the second set of values. In other h states, we cannot see such a distinction of all na values. Therefore, for the first case (h = 3 μm) we can choose the wavelength range (1.92-2.3 μm) to obtain a set of distinguishing peaks for the different values of refractive index na. This state was obtained when (R_1 =1.5 μm, R_2 =3 μm, t_m = 100nm) and we will therefore restrict ourselves to working within these limits to obtain the best results. The sensitivity of the wavelength for the best case in the figure when selecting the second set of peaks is about (9000nm/RIU) which are noteworthy values in this field and we will try to remain with the coefficients change (R_1, R_2, t_m) as an attempt to increase the wavelength sensitivity and study other measures used in the sensor field.

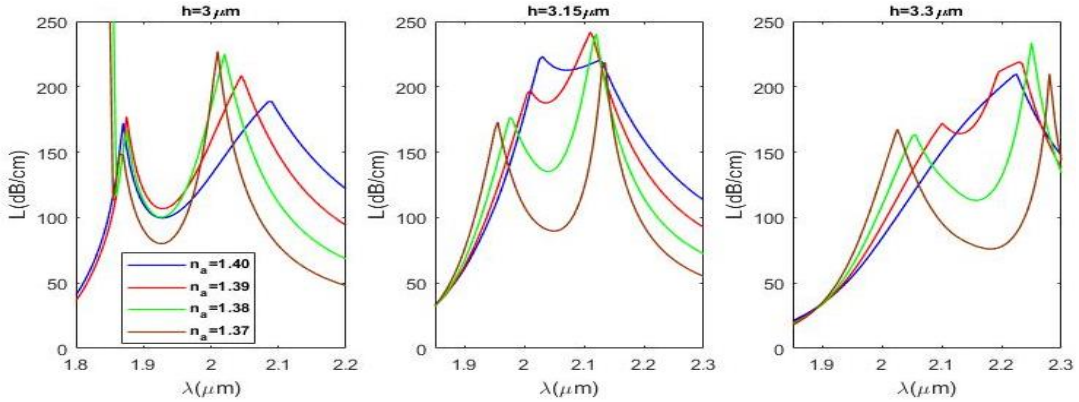

Figure 2. Confinement loss as a function wavelength of the analyte refractive indices n_a =1.37, 1.38, 1.39, 1.40 using different values of h

Figure 3 represents the relationship of the loss with the wavelength of the refractive indices (n_a =1.37, 1.38, 1.39, 1.40) using several values of the factor R_1, which represents the radius of the small circle that contains the analyte. We note from the figure that the best case is at (R_1 =1.5 μm), which gives the best spacing between the peaks and the highest value of the peaks. That is, it will be the best in terms of the wavelength sensitivity and amplitude sensitivity. Table 2 gives the sensitivity of the wavelength associated with all values of R_1.
lease make sure that the paper you submit is final and complete, that any copyright issues have been resolved, that the authors listed at the top of the chapter really are the final authors, and that you have not omitted any references. Following publication, it is not possible to alter or withdraw your paper on SpringerLink. Kindly note that we prefer the use of American English.

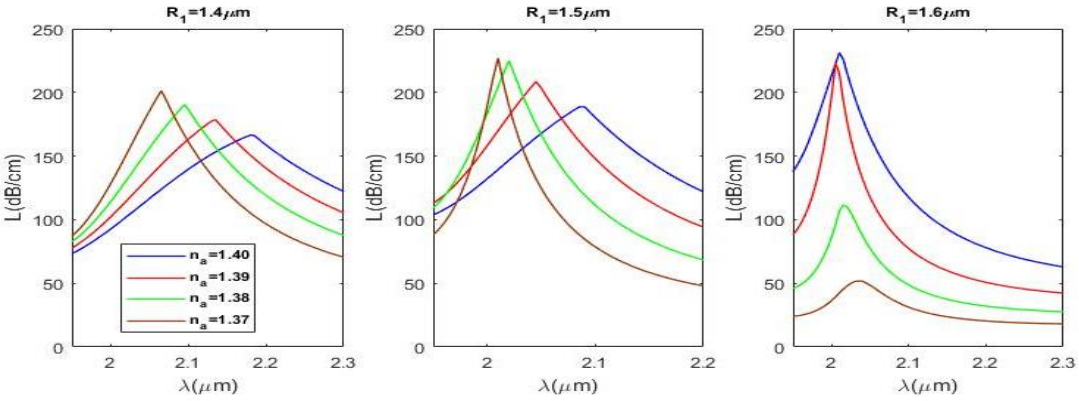

Figure 3. Confinement loss as a function wavelength of the analyte refractive indices n_a =1.37, 1.38, 1.39, 1.40 using different values of R_1

Note that the state (R_1 =1.4 μm) may have outperformed wavelength sensitivity values, but it would not be the best in the amplitude sensitivity field. However, the curves for different n_a values show different peaks that are further spaced with n_a increasing. That is, the sensitivity here increases for the greater n_a coefficients. With increasing R_1, the verification of the distinct peaks for the different n_a coefficients will not be achieved and we

will not be able accordingly to determine the refractive index of the liquid, where the state (R_1 = 1.6μm) shows a completely different behavior that will not be useful in the field of sensors.

Table 2. Wavelength sensitivity for different values of R_1, R2, t_m.

R_1 value in μm	Wavelength sensitivity (*nm*/RIU)	R_2 value in μm	Wavelength sensitivity (*nm*/RIU)	t_m value in *nm*	Wavelength sensitivity (*nm*/RIU)
1.4	6000,8000,9000	3	2000,5000,9000	80	1000,4000,6000
1.5	2000,5000,9000	3.15	6000,8000,10300	100	2000,5000,9000
1.6	1000,2000,4000	3.3	7000,8000,10000	120	4000,5000,8000

Figure 4 represents the loss relationship as a function of the wavelength of the refractive indexes (n_a =1.4, 1.39, 1.38, 1.37) using several values of R_2, which represents the radius of the large circles containing the air. It is evident from the figure that all the values of R_2 achieve distinct values that increase their spacing with an increase in the values of R_2, but this is accompanied by a decrease in the value of the peaks. State (R_2 =3 μm) shows the highest value and lowest spacing of peaks, noting that the start of the wavelength values indicates a peak near the left side that will seem to cause confusion when we choose (R_2 <3 μm). Generally, table (2) indicates the best wavelength sensitivity we get when (R_2 =3.3μm). Also here that the peaks show the beginning of the lowest refractive index n_a. And that the sensitivity increases for the greater n_a coefficients and that the wavelength that causes the peaks will shift to the left. Note here that the present behavior appears for the coefficients (R_1 =1.5 μm, t_m =100*nm*) and will change significantly as these coefficients change.

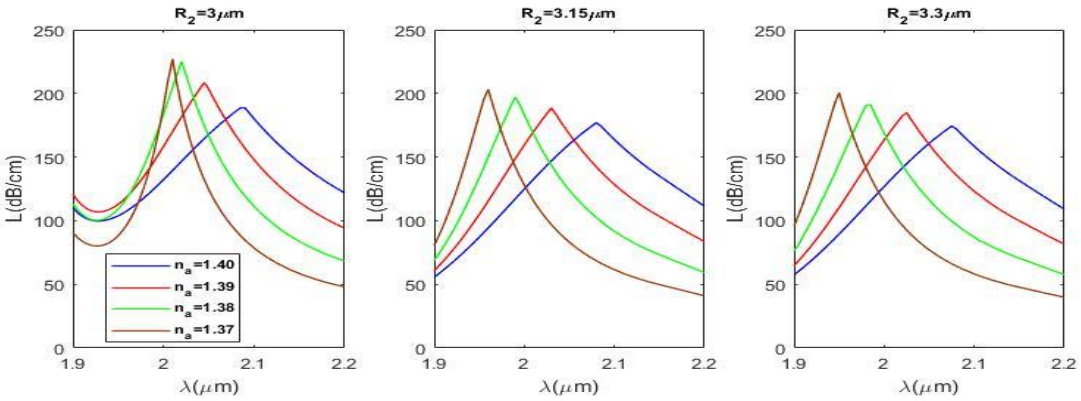

Figure 4. Confinement loss as a function wavelength of the analyte refractive indices n_a =1.37, 1.38, 1.39, 1.40 using different values of R_2

Figure 5 represents the relationship of the loss to the wavelength for different refractive factors (n_a =1.37, 1.38, 1.39, 1.40) using several values of the factor tm, which represents the thickness of the gold layer. We notice here that the best case for the values divergence is the state (t_m =100*nm*), with the fact that the case (t_m =80*nm*) gives the highest values for the peaks. At (t_m=120*nm*), note that the standard shape of the peaks that belong to the different n_a coefficients will disappear and one of the peaks will appear abnormally from their counterparts. We also note that for the case (t_m =100*nm*), the first peak appears at (λ ≈2.01 μm), for the case (t_m =80*nm*) the first peak appears at (λ ≈2.08 μm) and at (t_m = 120*nm*) we see that all the peaks shift to the left. It is clear from Table 2 that the best wavelength sensitivity is achieved at (t_m =100*nm*) and decreased with a change of t_m value. Table 3 represents the values of refractive index resolution obtained by adopting the changes during the simulation. It is clear that the lowest value occurs when (R_2 =3. 15 μm), (R_1 =1.5 μm) and (t_m =100*nm*) which is (9.7×10^{-6} *RIU*) at (n_a = 1.4) which corresponds to the highest wavelength sensitivity, which is (10300*nm* / *RIU*).

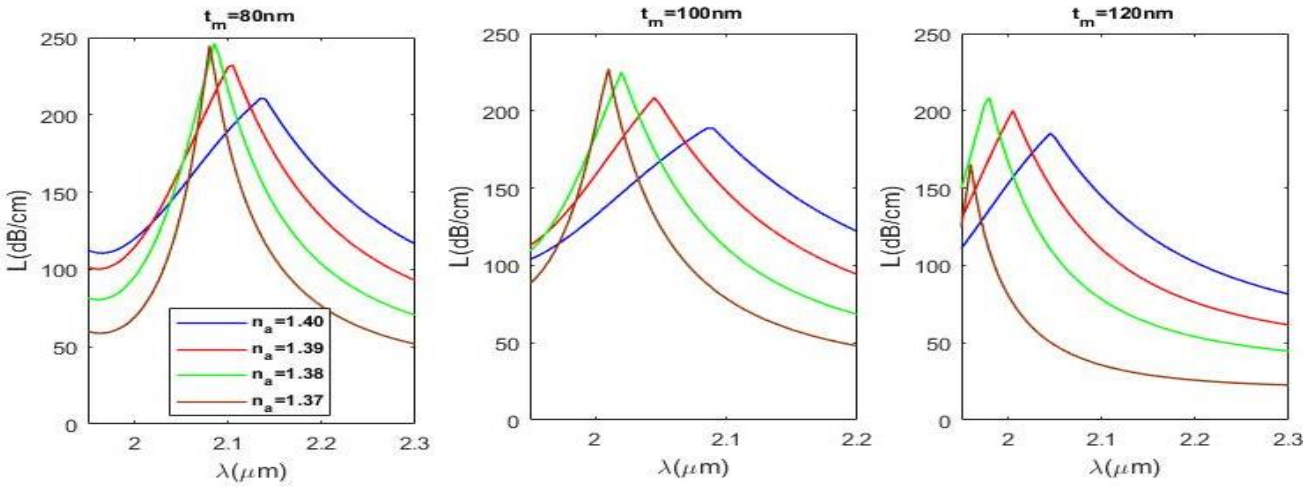

Figure 5. Confinement loss as a function wavelength of the analyte refractive indices n_a =1.37, 1.38, 1.39, 1.40 using different values of tm

Table 3. Refractive index resolution for different values of R_1, R_2, t_m

R_1 (μm)	Refractive index resolution (RIU)×10^{-5}	R_2 (μm)	Refractive index resolution (RIU) ×10^{-5}	t_m (*nm*)	Refractive index resolution (RIU)×10^{-5}
1.4	1.67, 1.25, 1.11	3	5, 2, 1.11	80	10, 2.5, 1.67
1.5	5, 2, 1.11	3.15	1.67, 1.25, 0.97	100	5, 2, 1.11
1.6	10, 5, 2.5	3.3	1.43,1.25, 1	120	2.5, 2, 1.25

Figure 6 represents the amplitude sensitivity as a function of the wavelength of the refractive indices (n_a=1.4, 1.39, 1.38, 1.37) for different values of R_1. When (R_1 =1.4 μm), all cases of n_a will achieve the maximum equal amplitude sensitivity, up to ($35RIU^{-1}$). When (R_1 =1.5 μm), the values differ for the different n_a values. From this we conclude that the case (R_1 =1.5 μm) is the best.

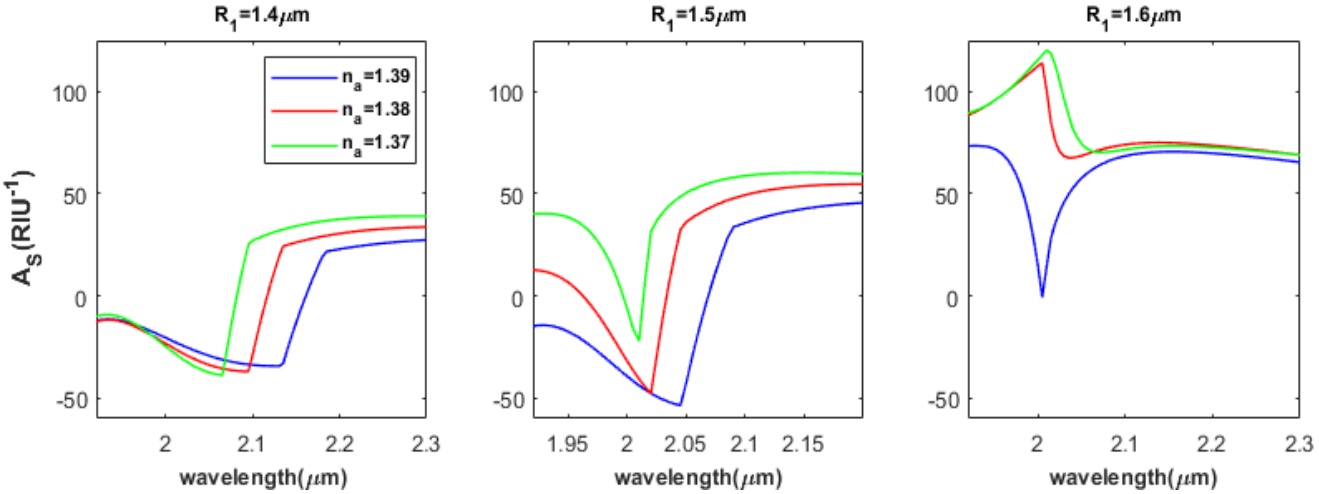

Figure 6. Amplitude sensitivity as a function wavelength of the analyte refractive indices n_a =1.37, 1.38, 1.39, 1.40 using different values of R_1

Figure 7 represents the amplitude sensitivity as a function of the wavelength of the refractive indexes (n_a =1.37, 1.38, 1.39, 1.40) for different values of R_2. We note from the figure that the case (R_2=3 μm) is less than the other two cases, and the case (R_2 =3.3 μm) is slightly superior to the case (R_2 =3.15μm). That is; the best designs are made by making (R_2 =3.3). Here, the amplitude sensitivity of the anlyte with the lowest refractive index will be the highest.

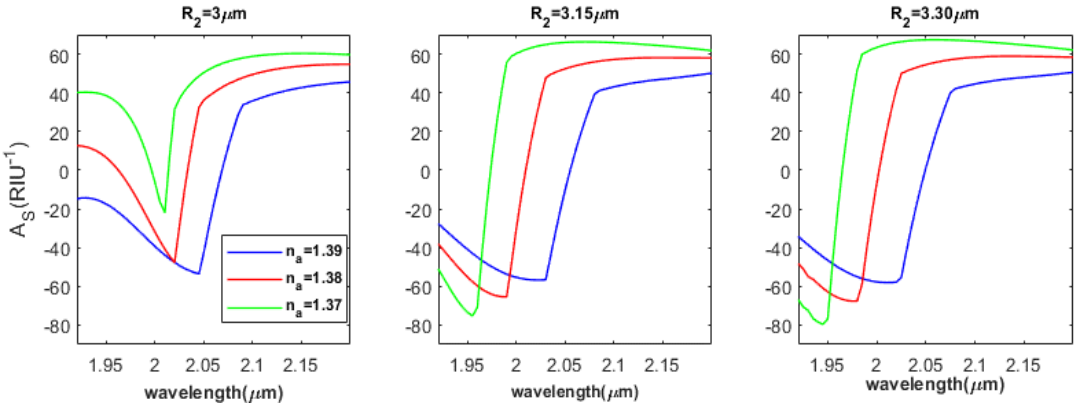

Figure 7. Amplitude sensitivity as a function wavelength of the analyte refractive indices n_a =1.37, 1.38, 1.39, 1.40 using different values of R_2

Figure 8 represents the amplitude sensitivity as a function of the wavelength of the refractive indexes (n_a =1.37, 1.38, 1.39, 1.40) for different values tm. We generally note that the higher the refractive index liquid is the higher amplitude sensitivity is achieved, and the amplitude sensitivity differences vary with the change of t_m. We note that the state (t_m =100nm) achieves better distinction in the peaks and thus can be adopted to maximize amplitude sensitivity.

Table 4 summarizes the maximum amplitude sensitivity achieved for all cases of the acceptable cases that can be adopted.

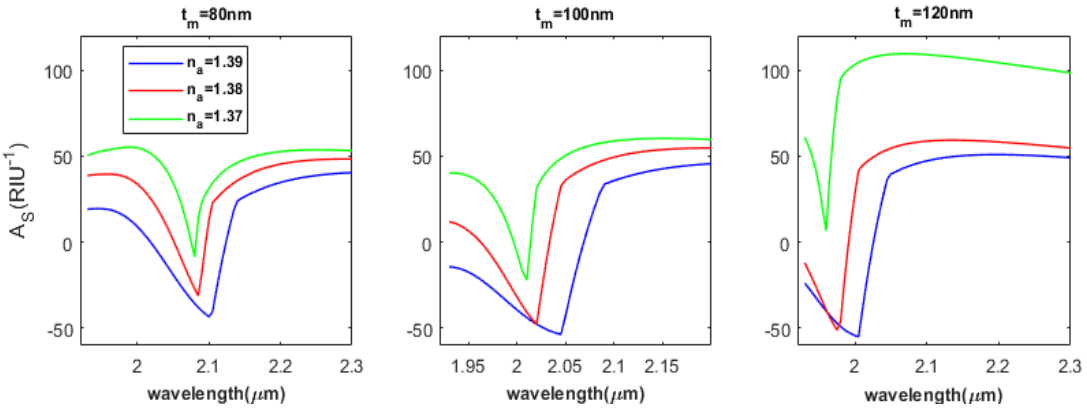

Figure .8. Amplitude sensitivity as a function wavelength of the analyte refractive indices n_a =1.37, 1.38, 1.39, 1.40 using different values of t_m

Table 4. Maximum amplitude sensitivity for different values of R_1, R_2, t_m.

$R_1(\mu m)$	$A_S(RIU^{-1})$	$R_2(\mu m)$	$A_S(RIU^{-1})$	$t_m(nm)$	$A_S(RIU^{-1})$
1.4	**35, 33, 33**	**3**	**22, 47, 56**	**80**	**9, 31, 43**
1.5	**18, 45, 56**	**3.15**	**75, 64, 54**	**100**	**22, 49, 54**
1.6	**---, --, 0**	**3.3**	**80, 68, 60**	**120**	**---, 51, 55**

Figure 9 represents the resonance wavelength relationship as a function of n_a for different states (R_1, R_2, t_m). We note from the figure that most relationships are semi-linear, as the closest relationship to linearity is the one that achieves the best sensor as long as the range n_a can be expanded to other values. When (R_1 =1.6μm) we see that the relationship is not linear and is completely rejected. Other cases of R_1 are not completely linear and it is possible to search near these values to achieve linearity. When (R_2 =3.3μm) the relationship is very close to be linear, and we noticed previously that it is the best case followed by (R_2 = 3.15μm) and then (R_2 = 3μm). All t_m cases are not completely linear but can be accepted to achieve optimum design conditions.

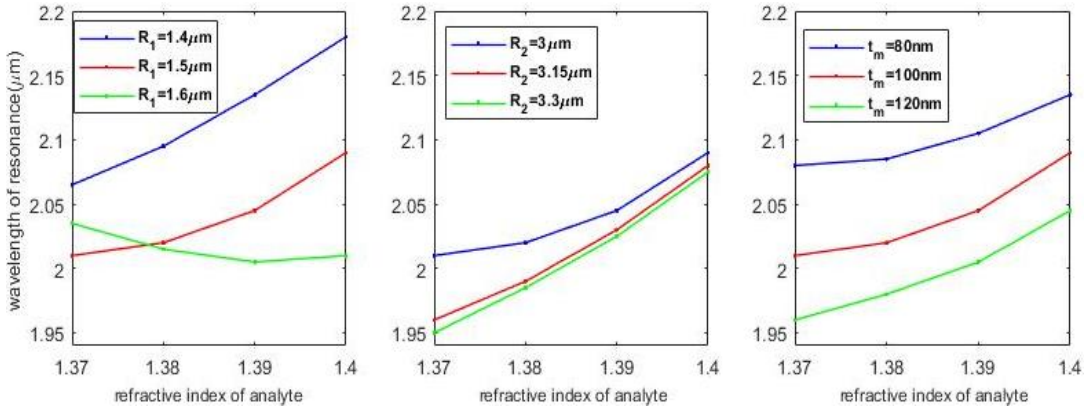

Figure 9. Wavelength of resonance as function of refractive index of analyte under the effects of R_1, R_2, t_m

5 Conclusions

The most important conclusion was achieved by obtaining the sensor property at (h =3μm) and its absence it at other values. The wavelength associated with the sensor property is in the range (1.93-2.3μm). When (R_1 =1.5μm, R_2 =3.3μm, t_m =100nm) the best results are achieved in the field of wavelength amplitude and amplitude sensitivity. The best sensor can be obtained within these values, which achieves the linearity between the wavelength of resonance and the refractive index of the liquid, since the linearity leads us to the possibility of using the sensor for other values of n_a outside the simulation values.

6. References

[1]A. A. Rifat Md. R. Hasan R. A. and H. Butt, "Photonic crystal fiber-based plasmonic biosensor with external sensing approach", Journal of Nanophotonics, Vol. 12, No. 1, 2017.
[2]A. A. Rifat, G. A. Mahdiraji, D. M. Chow, Y. G. Shee, R. Ahmed and F. R. M. Adikan, "Photonic Crystal Fiber-Based Surface Plasmon Resonance Sensor with Selective Analyte Channels and Graphene-Silver Deposited Core", Sensors Journal, Vol. 15, zno.5, 2015.
[3]A. Hassani and M. Skorobogatiy, "Photonic crystal fiber-based plasmonic sensors for the detection of biolayer thickness", Journal of the Optical Society of America B , Vol. 26, No. 8, 2009.
[4] M. Chauhan and V. K. Singh, "A fiber optic refractive index sensor using a high index layer of TiO2", AIP Conference Proceedings , Vol. 2220(020039), 2020.
[5]E. Haque, Md. A. Hossain, F. Ahmed and Y. Namihira, "Surface Plasmon Resonance Sensor Based on Modified D-Shaped Photonic Crystal Fiber for Wider Range of Refractive Index Detection", IEEE Sensors Journal , 1558-1748 (c), 2018.
[6]M. Erdmanis, D. Viegas, M. Hautakorpi, S. Novotny, J. L. Santos and H. Ludvigsen, "Comprehensive numerical analysis of a surface-plasmon-resonance sensor based on an H-shaped optical fiber", Optical Society of America journal , Vol. 19, No. 15, 2011.
[7]A. Hassani and M. Skorobogatiy, "Design of the Microstructured Optical Fiber-based Surface Plasmon Resonance sensors with enhanced microfluidics", Optical Society of America journal , Vol. 14, No. 124, (2006).
[8]M. S. Aruna Gandhi, S. Chu, K. Senthilnathan, P. R. Babu, K. Nakkeera, and Q. Li, "Recent Advances in Plasmonic Sensor-Based Fiber Optic Probes for Biological Applications", Applied Sciences journal , Vol. 9, No.5, 2019.
[9]A. K. Paul, G . k. Sarkar, B. S. Rahman and A. Khaleque, "Twin Core Photonic Crystal Fiber Plasmonic Refractive Index Sensor", IEEE Sensors Journal, Vol. 18, No.14, 2018.
[10] M. G. Somekh, and S. Pechprasarn, Surface plasmon, surface wave, and enhanced evanescent wave microscopy. Springer, 2017.
[11]A. Yasli and H. Ademgil, " Geometrical comparison of photonic crystal fiber-based surface plasmon resonance sensors", Optical Engineering journal, Vol. 57, No.3, 2018.
[12]R. K. Gangwar and V. K Singh, "Highly Sensitive Surface Plasmon Resonance Based D-Shaped Photonic Crystal Fiber Refractive Index Sensor", Plasmonics journal, Vol. 12, pp. 1367–1372, 2016.

[13]H. Li , Sh. Li , H. Chen, J. Li, G. An, J. Zi, "A Polarization Filter Based on Photonic Crystal Fiber with Asymmetry Around Gold-Coated Holes", Plasmonics journal, Vol. 11, pp. 103–108, 2015.
[14]Y. Li, "Plasmonic Optics: Theory and Applications", Spie Press Book, 2017.
[15] H. Y. Li, S. M. Zhou, J. Li, Y. L. Chen, S. Y. Wang, Z. C. Shen, L. Y. Chen, H. Liu, and X. X. Zhang. "Analysis of the Drude model in metallic films." *Applied optics, Vol.* 40, No. 34, pp.6307-6311, 2001.
[16]A. Vial et al., "Improved analytical fit of gold dispersion: application to the modeling of extinction spectra with a finite-difference time-domain method," Plasmonics journal, Vol. 10, PP. 1123–1131, 2005.
[17]A. D. Rakic , A. B. Djurisic, J. M. Elazar, and M. L. Majewski, "On the Performance of Graphene-Based D-Shaped Photonic Crystal Fibre Biosensor Using Surface Plasmon Resonance", Applied Optics, Vol. 37, No. 22, 2015.
[18]S. Das and V. K. Singh, "Refractive Index Sensor Based on Selectively Liquid Infiltrated Birefringent Photonic Crystal Fiber", Optik journal, Vol. 201, 163489, 2020.
[19]S. Das and V. K. Singh, "Dual Core Photonic Crystal Fiber based Surface Plasmon Resonance Biosensor", Optik journal, Vol. 170, pp. 400-408, 2018.
[20]X. Yang, Y. Lu, B. Liu, and J. Yao, "Analysis of graphene-based photonic crystal fiber sensor using birefringence and surface plasmon resonance," Plasmonics journal, Vol. 12, No. 2, pp. 489–496, 2017.